



HAL
open science

High-pressure A-site manganites: Structures and magnetic properties

E. Solana-Madruga, Angel Arévalo-López

► **To cite this version:**

E. Solana-Madruga, Angel Arévalo-López. High-pressure A-site manganites: Structures and magnetic properties. *Journal of Solid State Chemistry*, 2022, 315, pp.123470. 10.1016/j.jssc.2022.123470 . hal-03753964

HAL Id: hal-03753964

<https://cnrs.hal.science/hal-03753964>

Submitted on 19 Aug 2022

HAL is a multi-disciplinary open access archive for the deposit and dissemination of scientific research documents, whether they are published or not. The documents may come from teaching and research institutions in France or abroad, or from public or private research centers.

L'archive ouverte pluridisciplinaire **HAL**, est destinée au dépôt et à la diffusion de documents scientifiques de niveau recherche, publiés ou non, émanant des établissements d'enseignement et de recherche français ou étrangers, des laboratoires publics ou privés.

High-pressure A-site manganites: structures and magnetic properties.E. Solana-Madruga^{1*} and A. M. Arévalo-López^{2*}

1. Departamento de Química Inorgánica, Facultad CC. Químicas, Universidad Complutense de Madrid, Spain.
*elsolana@ucm.es
2. UMR-8181-UCCS- Unité de Catalyse et Chimie du Solide -Univ. Lille, CNRS, Centrale Lille, ENSCL, Univ. Artois, F-59000 Lille, France. *angel.arevalo-lopez@univ-lille.fr

Keywords: A-site manganites, magnetic frustration, perovskite, corundum, high pressure

Abstract:

Compounds of general formula ABO_3 are widely studied due to their versatility regarding chemical composition, structure and physical properties. The use of high-pressure and high-temperature synthesis method allows the introduction of small Mn^{2+} cation into the often-large *A* site, giving rise to the so-called *A*-site manganites, with a few exceptions to this rule. Polymorphism, structural features and magnetic properties of *A*-site manganites are revisited in this short review dedicated to Miguel A. Alario y Franco on his 80th birthday. We extend this dedication to John B. Goodenough and J. Paul Attfield on their 100th and 60th birthdays in recognition of their ground work. Happy birthday all three!

Introduction:

ABO_3 oxides are of wide interest in the search for new functional materials. Their chemical and structural versatility provides many possibilities in the design of materials with new or enhanced physical properties, which motivates a continuous production of new phases. A broad range of chemical compositions ^[1,2] and polymorphs are accessible by controlling the relative ionic radii of *A* and *B*-site cations, as defined by the Goldschmidt tolerance factor ($t = [(r_O+r_A)/\sqrt{2}(r_O+r_B)]$), ^[3] and the synthesis conditions. In particular, high-pressure and high-temperature (HPHT) synthesis method, which allows the stabilisation of metastable phases ruled by kinetics and hosting cations in unusual oxidation states or coordination environments, has lately raised interest in the growing family of the so-called *A*-site manganites as new functional materials.

A-site manganites are ABO_3 compounds where the *A* sites are occupied by Mn (generally 2+) cations. Partial substitution of *A* and/or *B*-site cations induces ordered derivatives with increased chemical, structural and functional complexity. The fast appearance of new phases with properties in the fields of magnetism, spintronics and multiferroics motivates this short review, where we aim to establish the relation between the chemical composition, structural details and magnetic properties of the known *A*-site manganites.

The article is organised in four different sections. The first two classify the high-pressure *A*-site manganites into their two known polymorphic families: perovskite- and corundum-related structures, with their different superstructures considering their *A/B* cation order. The third section briefly mentions some structural aspects to reconsider. Finally, we propose new directions in the design of novel materials.

A) Perovskite-related A-site manganites.

Cation order into the parent $MnBO_3$ "simple" perovskite structure (Pv) can be induced into *A* and/or *B* sublattices with 1:1, 1:2 and 1:3 order ratios, giving rise to the observed $AMnB_2O_6$ *A*-site ordered or $Mn_2BB'O_6$ *B*-site ordered double perovskites (DPv), $AMn_{0.5}Mn'_{0.5}BB'O_6$ double double perovskites (DDPv), $Mn_3MnB_2O_9$ triple perovskites (TPv) and $AMn_3B_4O_{12}$ quadruple perovskites (QPv). All known examples are summarised in the following sections, with a single case for simple Pv, one *A*- and twenty-one *B*-site ordered DPv, seventeen DDPv, two TPv and many QPv. The discussed structures are shown in Figure 1, where the occupational, rotational and displacive distortion modes relating each superstructure to the parent Pv structure are identified.

Complex magnetic properties are observed throughout the whole family, with coherent evolution of transition temperatures and magnetic moments within each superstructure type in terms of the number of unpaired electrons for *B*-site cations. Tables 1 and 2 summarise the main structural and magnetic features for *B*-site DPv and DDPv respectively.

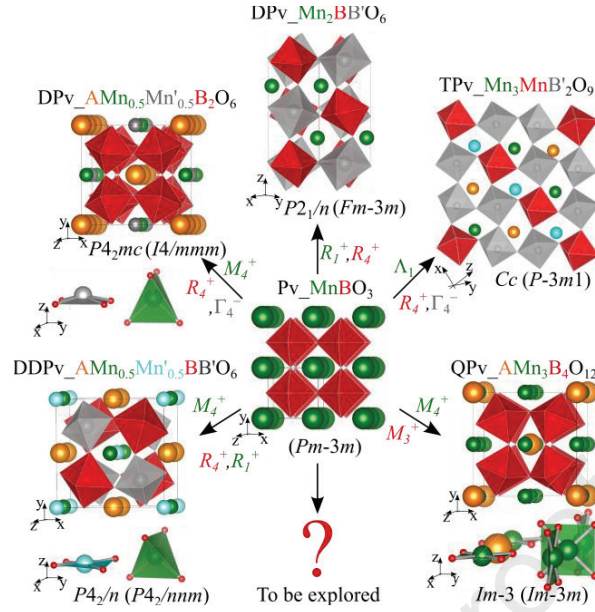


Figure 1. Perovskite related structures of A-site manganites. Cubic parent perovskite (Pv) in the middle, 1:1 cation orders at the A (DPv_{AMn_{0.5}Mn'_{0.5}B₂O₆}), B (DPv_{Mn₂BB'O₆}), A and B sites (DDPv_{AMn_{0.5}Mn'_{0.5}BB'O₆}); 1:2 order of B sublattice (TPv_{Mn₃MnB'₂O₉}) and 1:3 order of A sites (QPv_{AMn₃B₄O₁₂}). Colours in general compositions correspond to those of octahedra or spheres in the structures. A-site 4-fold coordination polyhedra are included below each superstructure for comparison. The labels in green, red, and grey relate the observed symmetry at room temperature to the parent Pv from occupational, rotational and displacive modes respectively, using a parent Pv with A sites at (½ ½ ½). Space groups in brackets show ideal symmetry for each superstructure attending only at the cation order.

1) Simple:

MnVO₃ is the unique simple A-site manganite that can be recovered from HPHT to ambient conditions. It crystallises with the *Pnma* Pv structure in a $\sqrt{2}a_p \times 2a_p \times \sqrt{2}a_p$ supercell, where $a_p \sim 3.8$ Å is the cell parameter of the cubic Pv. It shows spintronic properties arising from the combination of localised Mn²⁺ 3d⁵ and itinerant V⁴⁺ 3d¹ electrons.^[4] It is metallic between 2 and 300 K, while it shows a complex magnetic behaviour at low temperatures. Below $T_N = 50$ K, it develops an incommensurate magnetic structure with $[k_x 0 0]$ propagation vector and either a helical spin structure or a spin density wave of colinear moments with modulated amplitude (as shown in Figure 2a). Magnetic frustration factor $f = |\theta|/T_N \sim 3$ sets the starting point for the complex magnetism of A-site manganites.

Unquenchable high-pressure A-site simple perovskites have also been observed for MnSnO₃ and MnTiO₃ oxides.^[5] The three simple A-site perovskites show lower pressure corundum-related polymorphs which will be described in later sections.

2) Double:

Double perovskites are stabilised by 1:1 cation order into either A or B sites. Again, there is a single example of AMnB₂O₆ DPv A-site manganite: CaMnTi₂O₆.^[6] It crystallises with tetragonal symmetry in a $2a_p \times 2a_p \times 2a_p$ supercell (S.G. *P4₂mc*) and Ca and Mn order into columns along the c axis. Mn sites show alternated tetrahedral and square-planar coordination along its column, as shown in Figure 1. The cooperative off-centre of Ti in octahedral coordination via second-order Jahn-Teller and Mn shifts in the square planes, induce a ferroelectric – paraelectric transition at $T_C = 630$ K. Above this temperature, an order-disorder phase transition results in the non-isomorphic supergroup *P4₂/nmc* of the closely related A-site ordered DPv CaFeTi₂O₆.^[7] This makes CaMnTi₂O₆ the first ferroelectric compound with A-site columnar ordered DPv structure. It is also multiferroic, with a weak spin-polarisation coupling^[8] below its antiferromagnetic transition at $T_N = 10$ K. The low temperature magnetic phase (*P4₂'mc*) is predicted as a C-type AFM with $k = [0 0 0]$ propagation vector and collinear alignment of the spins along the c-axis, i.e. parallel to the columnar order and perpendicular to the square-planes.^[9] New improper ferroelectrics with different degrees of cation order can be accessed for instance in Ca_{2-x}Mn_xTi₂O₆.^[10]

Among B-site ordered Mn₂BB'O₆ *P2₁/n* double perovskites with $\sqrt{2}a_p \times \sqrt{2}a_p \times 2a_p$ supercell, a simple classification can be made considering the relative oxidation states of B/B' cations, i.e. 3+/5+, 2+/6+ and +7+. In all cases, the electronic configuration of B-site cations plays a key role in their magnetic properties, for which they can be further classified into dⁿ/d⁰(d¹⁰) and dⁿ/dⁿ materials. Two families of compounds with B²⁺ = Sb⁵⁺, Te⁶⁺ are reported in the first case (Mn₂ScSbO₆, Mn₂CrSbO₆, Mn₂CoTeO₆ and Mn₂MnTeO₆), all showing simple magnetic

behaviours with collinear antiferromagnetic (AFM) structures with $k = [0\ 0\ 0]$ or $[\frac{1}{2}\ 0\ \frac{1}{2}]$ propagation vectors (Figure 2b-top).^[11,12,13,14] The only exception is $\text{Mn}_2\text{FeSbO}_6$, where competing Mn-O-Mn and Mn-O-Fe $d^5 - d^5$ magnetic interactions frustrate the system into a complex helical spin structure with propagation vector $k = [0\ k_y\ 0]$ (shown in Figure 2b-bottom).^[15] The combination of paramagnetic cations into both B/B' sites is only reported for the “all transition metal” $B' = \text{Re}$ family. Strong magnetic interactions make $\text{Mn}_2\text{FeReO}_6$ a high temperature ferromagnet (FM) with $T_C = 520\ \text{K}$, and a colossal magnetoresistance switch induced by a low temperature spin reorientation transition.^[16,17] All other Mn_2BReO_6 belong to a complex series of frustrated magnets with B^{2+} and Re^{6+} perpendicular sublattices (Figure 2b-bottom right),^[18,19,20] except for $\text{Mn}_2\text{LiReO}_6$ DPv. This is the only case among all A -site manganites with B'/Re^{7+} and a giant magnetic coercivity due to magnetocrystalline anisotropy, enhanced by symmetry restrictions and without spin-orbit coupling.^[21] A special case is $\text{Mn}_2(\text{Fe}_{0.8}\text{Mo}_{0.2})\text{MoO}_6$,^[22] which was discovered as a line phase from a compositional modulation motivated from the parent $\text{Mn}_2\text{FeMoO}_6$ corundum-related phase. It exhibits a Fe-Mo ferrimagnetic (FiM) transition at $T_C = 194\ \text{K}$ and a Mn AFM at $T_N = 45\ \text{K}$. It demonstrates that both polymorphs can be tuned by slight variation of the composition.

$\text{MnRMnB}'\text{O}_6$ (where R stands for rare earth) DPv structures with $\text{Mn}^{2+}/\text{R}^{3+}$ disordered over the A sites and $\text{Mn}^{2+}/\text{B}'^{5+}$ ordered with a rock-salt pattern over the B sites are reported for $B' = \text{Sb}$ and Ta when R^{3+} cations are not large enough to induce further order into the A sublattice (*vide infra*).^[23,24,25] This evidences the polymorphism throughout two series of compounds, suggesting chemical pressure as a key factor on structural control. In a similar case, mixed A sites are also reported for CaMnMnWO_6 .^[24] As summarised in Table 1, the independent magnetic transitions are observed for Mn^{2+} and R^{3+} and a unique case of spin glass behaviour among all DPv A -site manganites for CaMnMnWO_6 , due to B -site geometric frustration.

Table 1. Main magnetic features of $\text{Mn}_2BB'\text{O}_6$ DPv with B/B' rock-salt order. S.G. $P2_1/n$, cell parameters $\sqrt{2}a_p \times \sqrt{2}a_p \times 2a_p$. Horizontal lines separate materials with $d^{10}(d^0)$ B' cations and d^n/d^n compounds at the top part. The lower half shows isostructural DPVs with mixed B or A occupancies.

B	B'	d_B		$d_{B'}$	T_N/T_C (K)	f	k_1	Other properties	Ref
		t_{2g}	e_g						
Sc	Sb	0	0	10	22	4.3	[000]	Polymorphism	11
Co	Te	5	2	10	27	---	[000]	Polymorphism	14
Mn	Te	3	2	10	36	5.1	$[\frac{1}{2}\ 0\ \frac{1}{2}]$	Polymorphism	20
Cr	Sb	3	0	10	55	4.0	$[\frac{1}{2}\ 0\ \frac{1}{2}]$	Polymorphism	12
Fe	Sb	3	2	10	60	3.0	[0 0.426 0]	Elliptical helix	15
Li	Re	0	0	0	109	1.2	[000]	Giant coercivity Polymorphism	21
Ni	Re	6	2	1	80	0.02	[000]	Spin rotation	20
Co	Re	5	2	1	94	3.6	$[\frac{1}{2}\ \frac{1}{2}\ 0]$	Semiconductor	19
Mn	Re	3	2	1	109	1.4	$[\frac{1}{2}\ \frac{1}{2}\ 0]$	Spin reorientation $T_{N2} = 40\ \text{K}$ to k_0 $T_{Re} = 99\ \text{K}$	18
Fe	Re	3	2	2	520	0.9		$T_{Mn} = 250\ \text{K}$ $T_{C3} = 75\ \text{K}$: spin reorientation and Magnetoresistance	16 17
$\text{Fe}_{0.8}\text{Mo}_{0.2}$	Mo	5	5/1	1	194	0.3	[000]	$T_{N2} = 45\ \text{K}$	22
A/A'	B/B'	e^-_A	d_B	$d_{B'}$	T_N/T_C (K)	f	k_1	Other properties	Ref
MnEu	MnSb	d^5/f^6	5	10	61	---	---	$T_{N2} = 38\ \text{K}$	23
MnGd	MnSb	d^5/f^7	5	10	67.5	0.5	---		23
CaMn	MnW	s^0/d^5	5	10	8	18	---	Spin glass Polymorphism	24
SmMn	MnTa	f^5/d^5	5	10	35	4.5	---	Polymorphism	24 25
EuMn	MnTa	f^6/d^5	5	10	26	---	---	$T_{C2} = 13\ \text{K}$	25
GdMn	MnTa	f^7/d^5	5	10	45	1.3	---	$T_{C2} = 20\ \text{K}$	25
YMn	MnTa	d^0/d^5	5	10	28	14	---	---	25
LuMn	MnTa	f^{14}/d^5	5	10	--	---	---	---	25
Mn	$\text{Mn}_{0.5}\text{Co}_{0.5}/\text{Te}$	5	5/7	10	31	---	$[\frac{1}{2}\ 0\ \frac{1}{2}]$	Magnetic phase coexistence	14
$\text{Mn}_{1.5}\text{Co}_{0.5}$	Co/Te	5/7	7	10	25	---	[000]	Polymorphism	14

* Missing values imply the compound is not fully studied.

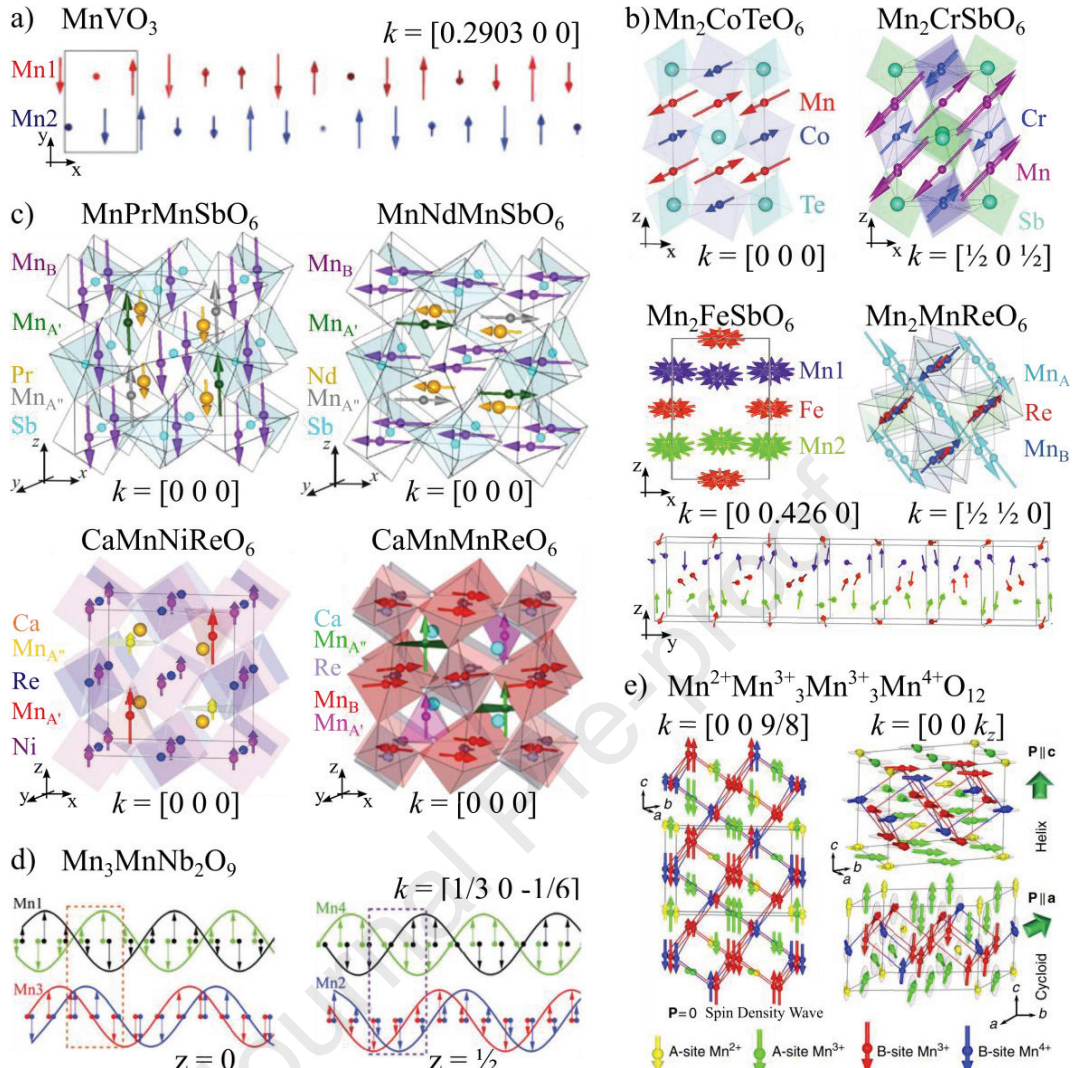


Figure 2. Representative examples of all types of reported magnetic structures for Pv (a), DPv (b), DDPv (c) and TPv (d) A-site manganites. e) shows the magnetic structures of Mn_2O_3 QPv. Figures adapted from references [4, 14, 15, 18, 31, 32, 34, 37, 53].

3) Double-double

Cation order into both *A* and *B* sites of the perovskite structure can happen into columnar (C), layered (L) or rock-salt (RS) arrangements. The combination of these three different patterns into both sublattices simultaneously allows 9 different types of doubly ordered perovskites. [2] Among them, only two combinations have ever been reported: layered/columnar patterns at *A/A'* sites with rock-salt order of *B/B'* cations. Layered and rock-salt orders are the most stable cation arrangements for *A* and *B* sublattices respectively and consequently there are many doubly ordered perovskites combining *L_A* + *RS_B*. [26,27,28,29,30] However, such order has not been observed with Mn in the layered position. The likely reason for this is the stress induced into the oxygen lattice due to Mn insertion. Nevertheless, the columnar order seems to favour small cations and thus it is much less stable among the usually large *A*-site cations, which makes it much rarer. Therefore, the amount of *C_A* DPv structures is scarce in comparison with *L_A* DPv. For the same reason, among doubly ordered perovskites, the *C_A* + *RS_B* combination had never been observed before the first *A*-site manganites with the so-called double double perovskite structure (DDPv), reported back in 2016. [23] As it happens in $\text{CaMnTi}_2\text{O}_6$ and $\text{CaFeTi}_2\text{O}_6$ (the only examples of *C_A* DPv up to date), [6,7] the combination of large (Ca^{2+} or R^{3+}) with the small (Fe^{2+} or Mn^{2+}) cations proved the major importance of having sufficiently different ionic radii over charge mismatch in the stabilisation of columnar cation order within the *A* sites, *ita vero* Ca and Mn are isovalent in this structure. The DDPv structure is notable for having 5 independent cation sites with 4 different coordination environments. As described in the previous section, Mn columns alternate tetrahedral and square-planar coordinations, revealing a close structural relation between these structures, with just an additional R^{1+} *B*-site ordering mode but with the same *A*-site and tilt M^{4+} and R^{4+} modes respectively as shown in Figure 1.

The DDPv structure has demonstrated a wide chemical and physical versatility in the last few years, where different cations could be stabilised within all 5 cation sites. This chemical flexibility is intrinsically coupled to a broad variety of magnetic properties, so compounds with ferro-, ferri-^[31] and antiferromagnetic behaviours have been reported with magnetic transitions at $42 \text{ K} < T_C < 560 \text{ K}$, including strong magnetic anisotropy and crystal field effects for MnMnSbO_6 ,^[32] spin reorientation transitions in $\text{MnNdMnB}'\text{O}_6$ ($B' = \text{Sb, Ta}$)^[23,25] and CaMnFeSbO_6 ,^[33] magnetoresistance as in $\text{CaMn}_{0.5}\text{Cu}_{0.5}\text{MnReO}_6$ and $\text{Ca}_x\text{Mn}_{2-x}\text{FeReO}_6$ solid solution for $0.17 < x < 1.73$ ^[34,35], and a cluster spin glass behaviour for CaMnFeTaO_6 .^[36] All reported DDPv show simple magnetic structures with propagation vector $k = [0 \ 0 \ 0]$. However, different observed spin arrangements can be summarised into antiparallel sublattices along the c or the a axis (Figure 2c-top) and parallel or perpendicular FM sublattices (Figure 2c-bottom). Order-disorder phase transitions are reported at high temperature in for instance CaMnMnWO_6 and RMnMnTaO_6 , resulting in the already described DPv.^[24,25] The main features of this family are condensed in Table 2.

Table 2. Main magnetic features of $\text{AMnBB}'\text{O}_6$ DDPv with A/Mn columnar and B/B' rock-salt orders. S.G. $P4_2/n$, cell parameters $2a_p \times 2a_p \times 2a_p$. Horizontal lines separate materials with $A = R / \text{Ca}^{f'}/s^0$ cations and B/B' 3+/5+ vs 2+/6+ oxidation states. The bottom part shows mixed A' cations and the only non-Mn based DDPv for comparison. Propagation vector in all studied cases $k_1 = [0 \ 0 \ 0]$.

A	B	B'	s/f _A	d _B		d _{B'}	T _N /T _C (K)	f	Other properties	Ref
				t _{2g}	e _g					
La	Mn	Sb	0	3	2	10	48	---	---	23, 32
Pr	Mn	Sb	2	3	2	10	89	---	T _{N2} = 75 K.	23, 32
Nd	Mn	Sb	3	3	2	10	76	1.1	Magnetic anisotropy T _{N2} = 42 K.	23, 32
Sm	Mn	Sb	5	3	2	10	80	1.6	Spin reorientation, Magnetic anisotropy.	23
La	Mn	Ta	0	3	2	10	49	3.6	T _{N2} = 39 K	25
Nd	Mn	Ta	3	3	2	10	65	2.2	T _{C2} = 40 K	25
									Spin reorientation, Magnetic anisotropy	
Sm	Mn	Ta	5	3	2	10	69	3.1	T _{C2} = 18 K	24,25
Ca	Cr	Sb	0	3	0	10	49	2.4	---	33
Ca	Fe	Sb	0	3	2	10	55	0.65	T _{C2} = 21 K,	33
									Spin reorientation	
Ca	Fe	Ta	0	3	2	10	51	1.4	T _{C2} = 20 K,	36
									Cluster spin glass	
Ca	Mn	W	0	3	2	10	45	4.4	Polymorphism	24
Ca	Ni	Re	0	6	2	1	152	0.99	Ferromagnetic	31
Ca	Co	Re	0	5	2	1	188	1	Ferrimagnetic	31
Ca	Mn	Re	0	3	2	1	120	---	T _{A'} = 100 K	34
Ca	Fe	Re	0	3	2	2	500	---	T _{A'} = 70 K	34
A	A'	B/B'	s _A	d _{A'}	d _B	d _{B'}	T _N /T _C (K)	f	Other properties	Ref
Ca	Mn _{0.5} Cu _{0.5}	Fe/Re	0	5/9	5	2	560	---	T _{A'} = 160 K	34
									Magnetoresistance	
Ca	Cu	Fe/Re	0	9	5	2	567	0.9	Butterfly-like magnetoresistance	a)

* Missing values imply the compound is not fully studied. a) Submitted.

4) Triple

A -site manganites with the triple perovskite structure have only been reported in 2021.^[37,38] $\text{Mn}_3\text{MnB}'_2\text{O}_9$ with $B' = \text{Nb}^{5+}$ and Ta^{5+} are obtained from high pressure and high temperature phase transformation of the $\text{Mn}_4\text{B}'_2\text{O}_9$ room pressure polymorphs, stabilising a 2:1 cation order among the B sites. This structure adopts a structural distortion from the archetype TPv $\text{Ba}_3\text{SrTa}_2\text{O}_9$ (S.G. $P-3m1$), where the combination of Λ_1 (2:1 cation order), R_4^+ (octahedral tilt) and Γ_4^- modes (displacive) results in independent crystallographic sites for all three A and B cations into Cc space group with a $\sqrt{6}a_p \times \sqrt{2}a_p \times 2\sqrt{3}a_p$ supercell. According to GKA rules,^[39] the expected AFM interactions cannot be satisfied for the Mn^{2+} spins at the B -site. Thus, a complex magnetic behaviour arises with three subsequent transitions on cooling. Below the first transition (T_N), these compounds adopt a collinear AFM structure with spins along the c axis and propagation vector $k = [0 \ 0 \ 0]$. The frustration of the B sites induces a modulation of the magnetic moments below T_M into a complex spin density wave with $k = [k_x \ 0 \ k_z]$. Both incommensurate components evolve continuously down to T_L , where they lock into a $k = [1/3 \ 0 \ -1/6]$. The value of

this propagation vector is dictated from the 2:1 *B*-site ordering and *A*-*B* frustrated interactions. A schematic representation of the complex SDW magnetic structure at low temperature is shown in Figure 2d. A detailed study on the frustrated magnetic interactions is included in the electronic supplementary information file for reference [37]. The room pressure multiferroic polymorphs are also recoverable under heating from the HPHT phase. The UV-Vis data shows a 25 % band gap reduction with respect to the $Mn_4B'_2O_9$ room pressure polymorphs due to the different connectivity of the $B'O_6$ octahedra in both structures.

5) Quadruple

Quadruple perovskites are an extended family of oxides [40,41,42] where $AA'_3B_4O_{12}$ exhibit 1:3 order of *A* and *A'* cations, which may also coexist with 1:1 order between *B* and *B'* sites into $AA'_3B_2B'_2O_{12}$ QDPv. [43] They mainly crystallise in the *Im*-3 cubic space group with a $2a_p \times 2a_p \times 2a_p$ supercell, but they often show lower symmetry due to charge-orbital orders. QPv *A*-site manganites are known with Mn^{3+} sitting at the square-planar *A'* sites only but also with aliovalent Mn occupying other cation positions. Among them, $A^+Mn^{3+}_3Mn^{3+}_2Mn^{4+}_2O_{12}$ (*A* = Na), [44] $A^{2+}Mn^{3+}_3Mn^{3+}_3Mn^{4+}_2O_{12}$ (*A* = Ca, Sr, Cd, Hg, Pb, Mn) [45,46,47,48,49] and $A^{3+}Mn^{3+}_3Mn^{3+}_4O_{12}$ (*A* = R, Bi) [50,51,52] compositions are reported. Note only $Mn^{2+}Mn^{3+}_3Mn^{3+}_3Mn^{4+}_2O_{12}$ includes Mn^{2+} at the highly coordinated *A* site, while *A'* sites are occupied by Mn^{3+} in all cases. QPvs are thus an exception to the usual 2+ valence of Mn in *A*-site manganites. Note also that $CaMn_7O_{12}$ can be obtained at room pressure conditions, resulting as well in an exception to the title compounds. The combination of mixed valence Mn into different crystallographic sites commonly induces complex magneto-orbital textures in these compounds, where ζ - Mn_2O_3 is notable as an “all Mn QPv” with a distortion down to triclinic symmetry. The more common cubic symmetry with *Im*-3 space group is shown in Figure 1 and the only-due-to-cation-ordering ideal space group *Im*-3*m* in brackets. ζ - Mn_2O_3 shows two intricate AFM structures below $T_N = 100$ K, combining a spin cycloid with a helical component (Figure 2e) which develops a ferroelectric polarisation. All of these occurs thanks to the combination of octahedral tilting, Jahn-Teller distortion and charge-orbital-spin ordering. [49,53]

The structural relation between Pv, *A* or *B* site ordered DPvs and DDPv is straightforward, given the related distortion modes, order ratios, tilt systems and coordination environments as described above and summarised in Figure 1. The different order ratio into the 1:2 *B*-site ordered TPvs is easily rationalised through the lambda mode relating the cubic Pv structure with the archetype TPv structure and further similar tilts and displacive modes. However, although the structural relation is undeniable, the 1:3 cation order into the QPv structure is not trivial to compare to 1:1 *A*-site ordering, even though some arguments were eventually reported. [54] The presence of a single crystallographic site for both *A* and *A'* sites with large cuboctahedral and square-planar coordinations respectively, in different stoichiometric proportions, requires the use of the M_4^+ mode to describe the cation order but results in *Im*-3*m* symmetry in the double supercell. Additional in-phase tilt mode M_3^+ , which also contrasts with the out-of-phase tilt R_4^+ observed in all other Pv-type *A*-site manganites, sets a further difference for QPvs. This means, M_4^+ mode is a second order parameter in the case of QPv where M_3^+ mode drives the 1:3 cation site splitting through octahedral tilt. Note the different symmetry relations in the *A*-DPv and DDPv structures yield to alternating square-planar and tetrahedral coordinations at the *A'* sites, in any case described as 2:1:1 order of *A*:*A'*:*A'* sites, but not as 3:1 *A*:*A'* as in the QPv structure.

B) Corundum-related A-site manganites.

As a rule of thumb, when the Goldschmidt tolerance factor $t < 0.75$ the corundum polymorph will be favoured. This just means that A and B sites have a similar size and it is the reason why many A_2O_3 compounds crystallise in this structure.

In parallel to the previous analysis regarding cation arrangements giving rise to ordered perovskite structures, cation order into the parent A_2O_3 disordered corundum structure (C) has been observed among A-site manganites into 1:1 ($MnBO_3$) and 1:2 (known as $Mn_4B_2O_9$ for the room pressure polymorph, but effectively $Mn_3(MnB_2)O_9$) ratios. Further order into doubly ordered $MnA'BB'O_6$ with 1:1 order into both A and B sublattices is also common when the chemical composition includes cations with large charge / size mismatches.

Regardless the degree of cation order into each sublattice, A-site Mn corundum related 1:1 ABO_3 compounds are usually referred to as $Mn_2BB'O_6$. Among them, compounds with B/B' cations similar in charge and ionic radii will result in disordered alternating (001) or (012) A/B layers into ilmenite (IL, $R-3$, Γ_2^+ occupational mode) [55] and LiNbO₃-type (LN, $R3c$, Γ_2^- occupational mode) [56] structures respectively. Another ordering is possible through the Γ_1^+ occupational mode. It results in the hypothetical $R32$ structure with ordering in dimers, but this has not yet been observed. Note that $Mn_4B_2O_9$ structure is the closest approach to such $R32$ structure, with Λ_2 occupational mode allowing a 2:1 Mn:B order that modifies octahedral connectivity every three (001) layers. This -hbc- sequence turns this structure into a bridge between hexagonal and cubic packing and thus between corundum- and perovskite-related phases via hexagonal perovskites. The three structures contain only two independent cation crystallographic sites. However, when charge and size difference between B and B' cations is larger, further order can be induced into the B sublattice of an ordered ilmenite (OIL) type structure. In this case, only three different cations are present but, due to symmetry relations, they are distributed over 4 independent crystallographic sites with space group $R3$. Note OIL shows alternating A/B (001) layers, while a similar double arrangement into ordered LiNbO₃ (OLN, $R3$) is also possible in the unique Co_2InSbO_6 [57] and not yet observed in A-site manganites. In the same way, partial substitution of Mn can also result in combined cation order into the A sublattice, giving rise to the so-called Ni₃TeO₆-type (NTO, $R3$) [58] structures, see Figure 3.

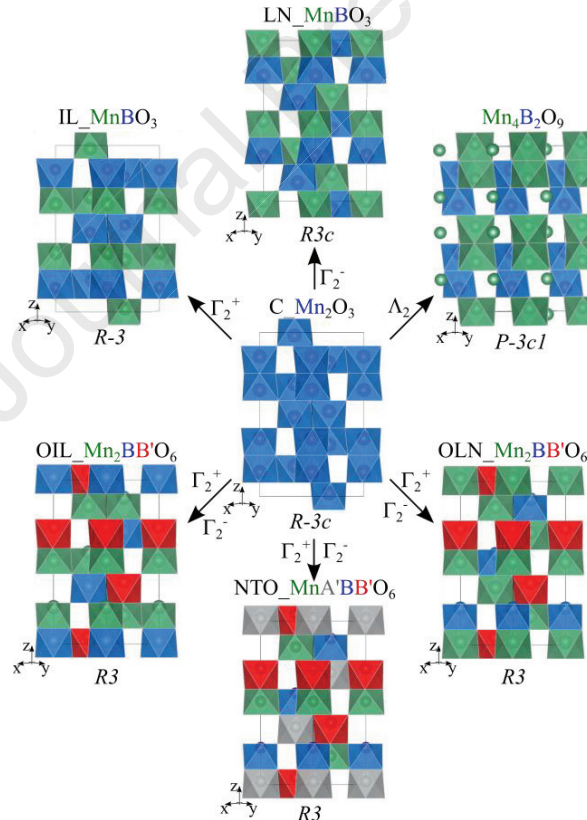


Figure 3. Corundum related structures of A-site manganites. Disordered parent corundum (C) in the middle, 1:1 cation orders into ilmenite (IL_ $MnBO_3$) and LiNbO₃-type (LN_ $MnBO_3$), 1:2 order into $Mn_4B_2O_9$ and additional order into both sublattices from 1:1 ordered derivatives into OIL_ $Mn_2BB'O_6$, OLN_ $Mn_2BB'O_6$ and Ni₃TeO₆-type structure (NTO_ $MnA'BB'O_6$). Colours in general compositions correspond to those of octahedra or spheres in the structures. Symmetry relations to the parent C structure are labelled.

A similar charge distribution comparison as that discussed for DPv phases reveals that most corundum-related $Mn_2BB'O_6$ oxides stabilise $3+/5+$ B/B' cations with IL ($B = Cr, Fe; B' = Sb$),^[12, 59] LN ($B = Fe; B' = Nb, Ta$),^[60] OIL ($B = In, Fe; B' = Sb, Mo$)^[61, 62] and NTO ($B = Sc, Fe; B' = Sb, Mo, W$) structures.^[11, 63, 64] Only Mn_3WO_6 and the $Mn_{3-x}Co_xTeO_6$ solid solution with $x \geq 1.5$ are reported with NTO-type structure and $2+/6+$ B/B' cations.^[14, 65] Also, a single example can be found with $+7+$ charge distribution at the B/B' sites of an OIL-type structure Mn_2LiReO_6 . It is the only member of the corundum-related A -site manganites with $B' = Re$ up to date.^[21] Due to the stacking of honeycomb and/or triangular magnetic sublattices along the c axis, all these compounds are largely frustrated, with complex magnetic phase diagrams including incommensurate helical/conical spin structures, temperature-dependent propagation vectors, lock-in phase transitions and even splitting k -vectors into competing ground states. The next subsections include further details on the magnetic properties of known corundum related A -site manganites as a function of their $A:B$ order ratio and are also summarised in Table 3. The magnetic behaviour of these compounds is due to stacking of triangular and honeycomb magnetic sublattices that give rise to strong magnetic frustration; representative examples of the magnetic structures are shown in Figure 4 and discussed in the following subsections.

1) Corundum (no order)

The closely related α - Fe_2O_3 and α - Cr_2O_3 are well-known text book examples of corundum antiferromagnets,^[66] However, α - Mn_2O_3 adopts a cubic bixbyite-type (C -type R_2O_3 , S.G. $Pbca$) structure. The Jahn-Teller effect of Mn^{3+} cations stabilises the oxygen-deficient fluorite structure rather than the corundum stacking at ambient conditions.^[67] It is only when using HPHT ($12 < P < 17$ GPa at 1200 K) that the initially identified as Mn_2O_3 corundum-type appears (ϵ - Mn_2O_3 , S.G. $R-3c$). Later on, this phase was properly identified as the charge ordered ϵ - $Mn^{2+}Mn^{4+}O_3$ ilmenite type structure (S.G. $R-3$)^[49, 68]. Provided the cation disorder from a strict chemical point of view, this phase is still included in this disordered section. Thus, no synthesis conditions have yet been reported to yield the formation of the $R-3c$ phase in kinetic conditions. Mn_2O_3 shows a rich P-T phase diagram discussed later on.

2) Simple (1:1 A:B order)

$MnTiO_3$ and $MnSnO_3$ are the only known non-distorted 1:1 ordered corundum derivative A -site manganites with "simple" ABO_3 chemical formula stabilising the two possible cation arrangements (IL- and LN-type structures). At ambient pressure, they crystallise with IL-type structure (I), and under 7 GPa they transform to a LN-type phase (II),^[69, 70] with canted antiferromagnetism below $T_N = 25$ and 50 K respectively and evidence for dielectric properties. A spin-flop transition at ~ 6 T turns $MnTiO_3$ -I into a magnetoelectric material with proposed ferrotoriodal order.^[71] The $MnTiO_3$ -II polymorph shows an unusual low field domain reorientation, which gives rise to weak ferromagnetic Dzyaloshinskii Moriya contributions perpendicular to the electric polarisation, thus turning $MnTiO_3$ -II into a multiferroic material.^[72]

$MnVO_3$ can be prepared as a distorted ilmenite (S.G. $P-1$) below 4 GPa.^[73] It presents a weak ferromagnetic transition with $T_N = 70$ K and $\theta = -430$ K, showing a larger frustration ($f = 6.1$) than its perovskite polymorph ($f \sim 3$) described in section A above.

3) Double (1:1 B:B' order)

As mentioned before, A -site manganites crystallise with IL ($R-3$) and LN ($R3c$) type structures for $Mn_2BB'O_6$ compositions with trivalent first row transition metals at the B sites and pentavalent cations at the B' sites. Despite the charge difference, B/B' cations with similar ionic radii are disordered and only a 1:1 arrangement is observed between Mn^{2+} (A) and $B(B')$ in alternating (001) or (012) layers respectively. Only four examples have been reported, where Sb^{5+} favours the IL order in Mn_2CrSbO_6 and Mn_2FeSbO_6 ^[12, 59] while transition metal Nb^{5+} and Ta^{5+} cations stabilise the LN structure for Mn_2FeNbO_6 and Mn_2FeTaO_6 .^[60] The different stacking of A and B octahedra arises from the smaller difference in averaged ionic radii for Mn^{2+} (0.83 Å) vs $Nb^{5+}(Ta^{5+})/Fe^{3+}$ (0.6425 Å) compared to Sb^{5+}/Fe^{3+} (0.6225 Å) or Sb^{5+}/Cr^{3+} (0.6075 Å),^[74] justifying the preferred location into A - B edge- / face-sharing octahedra respectively. The increasing number of unpaired electrons translates into progressively higher magnetic transition temperatures as summarised in Table 3. Magnetic structures are not studied in the LN samples, but the strong magnetic frustration of these systems with stacked honeycomb layers is observed in Mn_2BSbO_6 IL oxides. Stronger d^5 - d^6 AFM interactions between Mn^{2+} and Fe^{3+} stabilises a high temperature collinear magnetic structure with $k = [0\ 0\ 0]$, but an incommensurate helical spin structure is developed at lower temperatures with $k = [0\ 0\ k_z]$, where the spins lie in the ab plane (Figure 4a-left).^[59] Weaker d^3 - d^6 interactions and higher magnetic frustration index justify the continuous rotation of the spins in a T -dependent k_z for Mn_2CrSbO_6 .^[12] Coupled magnetoelectric properties were observed in Mn_2FeSbO_6 , supported by local lattice effects and suggesting accessibility to new multiferroic materials.^[59]

Preliminary studies on impurified Mn_2BSbO_6 with $B = Ga$ and Al ^[75] focus on structural features and show a pressure induced phase transition from IL to DPv type structure. Polymorphism in double corundum (DC) – double perovskite (DPv) A -site manganites has only been observed for $Mn_2BB'O_6$ with $B' = d^0/d^{10}$ cations, mainly antimonates, where high temperature has also been proven to trigger the reverse DPv to IL phase transition at room pressure conditions.^[12]

4) Triple $Mn_4B_2O_9$ (1:2 B order)

Room pressure polymorphs of $Mn_4B_2O_9$ ($B = Nb^{5+}, Ta^{5+}$) are well known multiferroic materials with space group $P-3c1$. Their composition can also be expressed as $Mn_3MnB'_2O_9$, suggesting a 1:2 order ratio between Mn and B' into the B sites. Two consecutive (001) honeycomb layers are formed by well-ordered Mn^{2+}/B^{5+} in octahedral coordination, where BO_6 octahedra are always connected via face sharing. One in three ab layers is purely formed of MnO_6 octahedra, supporting the 1:2 order in the B/B' sites of a triple corundum-related structure with ilmenite-type stacking, see Figure 3. The symmetry relation to the corundum structure requires a Λ_2 mode, reflecting the similar relation found between the cubic Pv and the TPv structure of $Mn_3MnB'_2O_9$ through mode Λ_1 . This TC polymorph is recoverable from the high pressure TPv phase by heating above 900 K. [38]

5) Doubly ordered $MnA'BB'O_6$ (1:1 A and/or B orders)

Combining cation order into (001) or (012) layers for A and/or B sublattices gives rise to R3 OIL and NTO-type structures for A -site manganites. They show four independent crystallographic sites for cations, thus giving rise to a total of 24 possible permutations when occupied by 4 different cations, but only 6 of those combinations are non-equivalent when considering symmetry arguments. Note that in $Mn_2BB'O_6$ oxides, 2/4 sites are occupied by Mn, thus leaving only three possible arrangements: OIL, OLN (with one existing compound, Co_2InSbO_6) [57] and NTO type structures, which could also be described as doubly-ordered ilmenite (DOIL) or $LiNbO_3$ -type (DOLN) structures.

Among $Mn_2BB'O_6$ oxides, three compounds are reported to crystallise with OIL structure, *i.e.* Mn_2InSbO_6 , Mn_2LiReO_6 and Mn_2FeMoO_6 . [61,21,62] These are chemically unique for different reasons: Mn_2InSbO_6 is the only non-polymorphic OIL synthesis product, Mn_2LiReO_6 is the only $Mn_2B^+B'^{7+}O_6$ and the only Re-based ordered corundum derivative, and Mn_2FeMoO_6 is notable as the only A -site manganite stabilised from an irreversible moderate temperature (450 K) cation rearrangement from a different ordered corundum derivative.

According to the expected magnetic frustration, Mn_2LiReO_6 shows no long-range magnetic order, with a spin cluster behaviour dominating the bulk magnetic properties. [21] Mn_2InSbO_6 shows three subsequent transitions where a simple ferrimagnetic structure ($k_1 = [0\ 0\ 0]$) turns into a T -dependent incommensurate helix ($k = [0\ 0\ k_2]$) which locks-in at low temperature ($k_3 = [0\ 0\ 1/8]$), [61] with $\sim 120^\circ$ spin angles between the three independent magnetic sites (see Figure 4b-right), reflecting the 3-fold symmetry of the hexagonal packing as often observed in NTO-type phases. [76] Regarding Mn_2FeMoO_6 , a collinear ferrimagnetic structure with all spins lying along the c axis with $k = [0\ 0\ 0]$ (Figure 4a-middle) is reported, its ordering temperature modulates with the degree of cation order. [62]

The more flexible NTO-type structure is reported for nine high pressure oxides with $MnA'BB'O_6$ general composition. Six of them are $Mn_2BB'O_6$ ($B = Sc^{3+}, Fe^{3+}, Fe^{2+}, Mn^{2+}$ and $B' = Sb^{5+}, Nb^{5+}, Ta^{5+}, Mo^{5+}, W^{6+}$) [11,63,64,65,77] and the other three correspond to the $Mn_{3-x}Co_xTeO_6$ ($x = 1.5, 2, 2.5$) solid solution. [14] Among $Mn_2BB'O_6$, the only clear doubly ordered corundum with a chemically based NTO structure as described above are $Mn_2ScB'O_6$ ($B' = Sb, Nb, Ta$). A site-selective antisite disorder between one Mn and Sc sites induces a weak ferromagnetic moment in all three samples ($T_C = 42, 53$ and 50 K respectively) into the collinear AFM structure, confirmed from neutron diffraction for Mn_2ScSbO_6 . [11] Metamagnetism is induced in Mn_2ScTaO_6 for $H_C > 0.5$ T, although the origin of this transition is not clear. [77] The accurate cation arrangements for the other three compounds are discussed in the next section.

Despite the presence of paramagnetic cations into all 4 sites, Mn_2FeMoO_6 shows a simple magnetic behaviour, with a collinear $k = [0\ 0\ 0]$ structure with spins parallel to the c axis, like that of the OIL modification. [63] Mn_2FeWO_6 shows a metamagnetic hysteretic behaviour explained in terms of competing (calculated) collinear structures, though a more complex non-collinear magnetic structure is also suggested. [64] A different behaviour is observed from experimental data on Mn_3WO_6 , with an incommensurate conical magnetic structure (partially shown in Figure 4a-right) which satellites are consistent with coexisting $k_1 = [0\ 0\ 3/2]$ and $k_2 = [0\ 0\ 0.3]$, thus combining the incommensurate and locked features usually observed in honeycomb/triangular lattices. [65]

Concerning the $Mn_{3-x}Co_xTeO_6$ ($x = 1.5, 2, 2.5$) solid solution, [14] their magnetic behaviour shows coexisting $k = [0\ 0\ k_2]$ and $[0\ 0\ 0]$, modulating the magnetic moments into an incommensurate elliptical helix (Figure 4b-bottom) in all cases. The coherent evolution of their transition temperatures and the absence of thermal dependence for k_z , in contrast to Co_3TeO_6 , is explained in terms of progressively weakened $d^{\delta}-d^{\delta'}$ superexchange interactions and less effective direct orbital overlap according to GKA rules. [39]

Note all these OIL and NTO-type phases, along with the possible OLN arrangement, are polar structures with cation shifts along the c axis inducing potential multiferroicity when the magnetic moments lie in the perpendicular ab plane (as in helical k_z structures). The spontaneous polarisation and magnetoelectric coupling are estimated for most of them from point charge or DFT calculations, and confirmed by second harmonic generation or pyroelectric current measurements.

Table 3. Main magnetic features of $Mn_2BB'O_6$ DC phases. The lower part of the table shows compounds in the solid solution $Mn_{3-x}Co_xTeO_6$ with mixed A sites.

B	B'	Struct./S.G.	d_B		$d_{B'}$	T_N (K)	k_1	f	Other properties	Ref
			t_{2g}	e_g						
Fe	Sb	IL / $R-3$	3	2	10	260	[000]	1.8	Giant MEC at T_{N1} $k_2 = [000.07]$ $T_{N2} = 50$ K Relaxor AFE < 650 K	59
Cr	Sb	IL / $R-3$	3	0	10	60	$[00k_z]$	3.3	T-dependent k_z	12
Sc	Sb	NTO / $R3$	0	0	10	42	[000]	3.3	wFM from site selective antite	11
In	Sb	OIL / $R3$	5	5	10	38	[000]	4.2	$<T_{N2} = 17$ K: $[00k_z]$ $T_{N3} = 8$ K: lock-in $[0\ 0\ \frac{1}{8}]$	61
Sc	Nb	NTO / $R3$	0	0	0	53	---	3.9	Insulator	77
Sc	Ta	NTO / $R3$	0	0	0	50	---	3.9	Insulator. Metamagn. $H_c = 0.5$ T	77
Mn	W	NTO / $R3$	3	2	0	58	$[0\ 0\ 3/2] +$ $[0\ 0\ 0.3]$	4.8	$T_{N2} = 20$ K: $[00k_z]$ conical	65
Fe	W	NTO / $R3$	3	2	1	75	[000]	---	Colinear // c	64
Fe	Nb	LN / $R3c$	3	2	0	90	---	---	Polar	60
Fe	Ta	LN / $R3c$	3	2	0	80	---	2.6	Polar	60
Fe	Mo	NTO / $R3$	3	2	1	337	[000]	0.7	Colinear // c	63
Fe	Mo	OIL / $R3$	3	2	1	229	[000]	---	Colinear // c	62
Li	Re	OIL / $R3$	0	0	0	46	---	4.3	Cluster spin glass	21
A/A'	B/B'	Struct./S.G.	d_A	d_B	$d_{B'}$	T_N (K)	k_1	f	Other properties	Ref
$Mn_{1.5}Co_{0.5}$	CoTe	NTO / $R3$	5/7	7	10	67	$[0\ 0\ 0.080]$	---	Elliptical helix	14
MnCo	CoTe	NTO / $R3$	5/7	7	10	72	$[0\ 0\ 0.094]$	---	Elliptical helix	14
$Mn_{0.5}Co_{1.5}$	CoTe	NTO / $R3$	5/7	7	10	66	$[0\ 0\ 0.117]$	---	Elliptical helix	14

* Missing values imply the compound is not fully studied

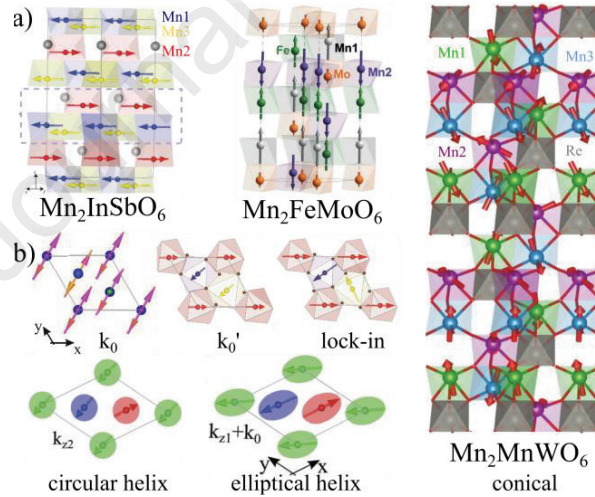


Figure 4. Representative examples of all types of reported magnetic structures for corundum related high pressure A-site manganites. a) $[110]$ projection of the nuclear unit cell showing representative examples with the spins lying on the ab plane (left) or along the c axis (middle). Right panel shows part of the conical magnetic structure only reported for Mn_2MnWO_6 . b) top view of magnetic structures with commensurate propagation vector (top) and consecutive spin angles 0° , $0^\circ < \theta < 180^\circ$ and 120° . Bottom panel shows incommensurate structures with circular and elliptical helix models. Figures adapted from references [11, 14, 61, 62, 65].

C) Structural aspects to reconsider.

From the chemical point of view, the cation distribution in Mn_2FeMoO_6 and Mn_2FeWO_6 , with alternating (012) Mn and 1:1 Fe:Mo(W) layers, ^[63,64] actually describes an OLN structure. It is reasonable that OLN and OIL modifications are very close in energy, enabling their formation in similar synthesis conditions or their

interconversion under soft conditions, as observed in $\text{Mn}_2\text{FeMoO}_6$,^[62] in simple MnBO_3 IL to LN polymorphs or the OIL to OLN in $\text{Co}_2\text{InSbO}_6$, triggered by thermal relaxation.^[57] In the case of Mn_2FeWO_6 , the authors highlight that Mn/Fe antisite is not well characterised in the preliminary study, and this could involve “an effect on the magnetic properties”. In the reported structure, antisite exchange of Fe with the so-called Mn1 or Mn2 sites would turn the OLN into an actual NTO or an OIL phase, respectively. Only a full structural characterisation from neutron diffraction will answer this ambiguity and reveal the magnetic structures that may explain the bulk magnetic behaviour of this phase. Note $\text{Mn}_2\text{ScNbO}_6$ and $\text{Mn}_2\text{ScTaO}_6$, also reported as NTO-type structures, show up to 40% antisite disorder between Sc and one Mn, thus lying in the limit between NTO and OIL structures.^[77] The reported field induced transition is likely due to different magnetic domains with similar energy in inhomogeneous samples.

Mn_3WO_6 is reported as NTO-type, this is a comprehensible mistake, considering that Ni_3TeO_6 itself shows a similar OIL cationic arrangement.^[58] Regarding the $\text{Mn}_{3-x}\text{Co}_x\text{TeO}_6$ solid solution, different proportions of mixed occupancies involve the intrinsic double order into the NTO-type structure, even though a clear site preference is observed for Mn in the Te (00l) layer, suggesting the OIL is more stable than the OLN arrangement in these compounds.

D) Perspectives.

HPHT synthesis is confirmed from all previous materials as an essential tool to access many new polymorphic compounds among A-site manganites, with different types of cation order and physical properties. Some of them deserve a special attention regarding future possibilities:

1) Mn_2O_3 is remarkable as the most polymorphic among A-site manganites: starting from the α - Mn_2O_3 (S.G. *Ia-3*) room pressure bixbyite phase, it transforms at low temperature ($T < 300$ K) to β - Mn_2O_3 (S.G. *Pbca*) and the metastable γ - Mn_2O_3 (S.G. *I4/amd*) obtained by soft methods. It presents three high pressure transformations to the ϵ - Mn_2O_3 (Ilmenite type, S.G. *R-3*) between $12 < P < 17$ GPa and $1200 < T < 1700$ K. It also transforms to ζ - Mn_2O_3 (QPv type, S.G. *Im-3*) between $18 < P < 23$ GPa and $900 < T < 1500$ K and to a post-perovskite structure above 28 GPa, δ - Mn_2O_3 (S.G. *Cmcm*). Under extreme pressure conditions, unquenchable θ - Mn_2O_3 (orthorhombic) and η - Mn_2O_3 (perovskite S.G. *Pnma*) coexist with the post-perovskite structure. Such a rich P-T phase diagram in the simplest chemical composition among A-site manganites suggests many new HPHT phases could be found for more complex chemical compositions.

2) $\text{Mn}_{11}\text{Ta}_4\text{O}_{21}$ ^[78] was found as an overstoichiometric ($\text{Mn}_8(\text{Mn}_3\text{Ta}_4)\text{O}_{21}$) hexagonal perovskite (HPv) with a $14\text{H}-(\text{cchchch})_2$ sequence, similar to those of the related 14H high pressure HPvs BaVO_3 and BaCrO_3 .^[79,80] At $T_{N1} = 88$ K AFM ordering develops and below $T_{N2} = 56$ K a spin reorientation originates a ferromagnetic component on additional A-site Mn cations, also inducing a magneto-structural coupling with possible magnetoelectric effect. The finding of this first hexagonal A-site manganite (HAM) suggests the accessibility to other related compounds. New HAM samples may be found and HPHT phase transitions to cubic polymorphs can be expected, as observed in other HPvs.^[81] Moreover, the close structural relation between $\text{Mn}_4\text{B}_2\text{O}_9$ and $\text{Mn}_3\text{MnB}'_2\text{O}_9$ structures, as a TC (with hexagonal close packing) and TPv structures with 1:2 B-site order suggests many new compounds with TC, TPv and HPv structures may be accessible through HPHT synthesis.

3) Mn_3TeO_6 ^[13] and $\text{Mn}_3\text{MnB}'_2\text{O}_9$ ^[37,38] oxides have shown interconversion between their respective room and high-pressure polymorphs. In both cases, a reduced band gap was observed for the HP phase, due to the lower connectivity of $\text{B}'\text{O}_6$ octahedra. Band gap tuning is thus expected for other polymorphic compounds, allowing for manipulation of their optical properties.

4) CaMnMnWO_6 DPv^[24] shows a spin glass behaviour from B-site geometric frustration. This finding suggests accessibility to several new compounds with frustrated magnetic properties never observed among A-site manganites. For instance, substitution of Mn^{2+} ($S = 5/2$) by Cu^{2+} ($S = 1/2$) may induce quantum spin liquid behaviour.

5) Among cation ordered corundum related phases, OLN type structure has not yet been observed for A-site manganites. However, it has been recently reported for the related Co-based HPHT $\text{Co}_2\text{InSbO}_6$.^[57] Under HP conditions, this compound adopts a new *R3* structure deriving from cation order of a never observed hypothetical *R32* corundum derivative, where *A/A'* cations locate at face-sharing octahedra. A two-step phase transition is triggered by temperature under room pressure conditions, giving rise to two new OLN phases. This finding, together with precedents of high temperature phase transitions in polymorphic A-site manganites and a rich history of similar transitions for other HPHT materials, suggests accessibility to OLN polymorphs for $\text{Mn}_2\text{BB}'\text{O}_6$ samples. Other cationic rearrangements may also be observed from high temperature phase transitions of known OIL phases into new OLN or NTO structures. This will of course produce dramatic changes in their magnetic properties.

6) Interplay between corundum- and perovskite – related polymorphs is common among A-site manganites with d^0 or d^{10} B' cations as a function of pressure and temperature conditions, for instance $\text{Mn}_{3-x}\text{Co}_x\text{TeO}_6$,^[13,14] Mn_2BSbO_6 ,^[11,12,15,59] and $\text{Mn}_2\text{LiReO}_6$.^[21] Temperature control has also proven essential to induce cation order-disorder phase transitions between DPv and DDPv structures, as in RMnMnTaO_6 .^[24] Cation rearrangement also gives access to phase transitions between different corundum-related superstructures, triggered by thermal relaxation in $\text{Mn}_2\text{FeMoO}_6$.^[62] Small compositional modifications in $\text{Mn}_2\text{FeMoO}_6$ allowed the stabilisation of a perovskite-related polymorph for $\text{Mn}_2(\text{Fe}_{0.8}\text{Mo}_{0.2})\text{MoO}_6$.^[22] This single case, in the middle of a rich playground for

polymorphism, suggests accessibility to several new functional oxides with tuned properties from slight chemical modification.

7) MnTaO₂N is the single example of a HP A-site manganite oxynitride.^[82] Other polyanionic A-site manganites should be expected, allowing for tunability of cation charge and thus inducing further degrees of freedom for potential spin, charge and orbital orders in new multifunctional materials with modulated spin (SDW) and charge density wave (CDW) structures.

In conclusion, new unknown polymorphs may be found for A-site manganites under HPHT conditions, such as hexagonal perovskites, different combinations of order into A and B sublattices in new DDPv structures, combined cation order into AMn₃B₂B'₂O₁₂ QDPvs or Mn₂AMnB'₂O₉ DTPv, layered or oxygen deficient perovskite phases, including brownmillerite-type, Ruddlesden-Popper, Dion-Jacobson or Aurivillius type structures. Among corundum related phases, new cationic rearrangements are also possible, with unknown OLN, R32 and its ordered derivatives yet to be found. Polymorphism, only found among B' d⁰/d¹⁰ cations up to date is also expected to provide new compounds among these oxides. Further compositions with mixed anions are also expected. The already success on finding new materials with a variety of properties and compositions advocates to continue the search on this prolific playground of HPHT A-site manganites where many new compounds are envisaged.

Acknowledgments

ESM thanks for financial support to the MICINN of Spain, project PID2020-112848RB-C21.

AMAL thanks support from the ANR of France, AMANTS project 19-CE08-0002-01.

References

- ¹ S. Vasala, M. Karppinen, *Prog. Solid State Chem.* 2015, **43**, 1-36.
- ² G. King, P. M. Woodward, *J. Mater. Chem.* 2010, **20**, 5785-5796.
- ³ V. M. Goldschmidt, *Mat-Naturu Kl*, 1926, Vol. **2**, 117.
- ⁴ M. Markkula, A. M. Arevalo-Lopez, A. Kusmartseva, J. A. Rodgers, C. Ritter, H. Wu, J. P. Attfield, *Phys. Rev. B*, 2011, **84**, 94450.
- ⁵ K. Leinenweber, W. Utsumi, Y. Tsuchida, T. Yagi, K. Kurita, *Phys. Chem. Minerals*, 1991, **18**, 244–250.
- ⁶ A. Aimi, D. Mori, K. Hiraki, T. Takahashi, Y. Jin Shan, Y. Shirako, J. Zhou, Y. Inaguma, *Chem. Mater.* 2014, **26**, 2601-2608
- ⁷ K. Leinenweber, J. Parise, *J. Solid State Chem.* 1995, **114**, 277–281.
- ⁸ G. Gou, N. Charles, J. Shi, J. M. Rondinelli, *Inorg. Chem.* 2017, **56**, 11854–11861.
- ⁹ J. Herrero-Martín, J. Ruiz-Fuertes, T. Bernert, M. Koch-Müller, E. Hausühl, J. L. García-Muñoz, *Phys. Rev. B*, 2018, **97**, 235129
- ¹⁰ Z. Li, Y. Cho, X. Li, X. Li, A. Aimi, Y. Inaguma, J. A. Alonso, M. T. Fernandez-Diaz, J. Yan, M. C. Downer, G. Henkelman, J. B. Goodenough, J. Zhou, *J. Am. Chem. Soc.* 2018, **140**, 2214–2220.
- ¹¹ E. Solana-Madruga, A. J. Dos santos-García, A. M. Arévalo-López, D. Ávila-Brande, C. Ritter, J. P. Attfield, R. Sáez-Puche, *Dalton Trans.*, 2015, **44**, 20441-20448.
- ¹² A. J. Dos santos-García, E. Solana-Madruga, C. Ritter, D. Ávila-Brande, O. Fabelo, R. Sáez-Puche, *Dalton Trans.*, 2015, **44**, 10665-10672.
- ¹³ Á. M. Arévalo-López, E. Solana-Madruga, C. Aguilar-Maldonado, C. Ritter, O. Mentré, J. P. Attfield, *Chem. Commun.*, 2019, **55**, 14470-14473.
- ¹⁴ E. Solana-Madruga, C. Aguilar-Maldonado, C. Ritter, M. Huvé, O. Mentré, J. P. Attfield, Á. M. Arévalo-López, *Chem. Commun.*, 2021, **57**, 2511-2514.
- ¹⁵ A J Dos Santos-García, C Ritter, E Solana-Madruga, R Sáez-Puche, *J. Phys.: Condens. Matter*, 2013, **25**, 206004.
- ¹⁶ M.Rong Li, M. Retuerto, Z. Deng, P. W. Stephens, M. Croft, Q. Huang, H. Wu, X. Deng, G. Kotliar, J. Sánchez-Benítez, J. Hadermann, D. Walker, M. Greenblatt, *Angew. Chem. Int. Ed.* 2015, **54**, 12069–12073.
- ¹⁷ A. M. Arévalo-López, G. M. McNally, J. P. Attfield, *Angew. Chem. Int. Ed.* 2015, **54**, 12074–12077.
- ¹⁸ A. M. Arévalo-López, F. Stegemann, J. P. Attfield, *Chem. Commun.*, 2016, **52**, 5558-5560.
- ¹⁹ C. E. Frank, E. E. McCabe, F. Orlandi, P. Manuel, X. Tan, Z. Deng, M. Croft, V. Cascos, T. Emge, H. L. Feng, S. Lapidus, C. Jin, M. X. Wu, M. R. Li, S. Ehrlich, S. Khalid, N. Quackenbush, S. Yu, D. Walker, M. Greenblatt, *Chem. Commun.*, 2019, **55**, 3331-3334.
- ²⁰ E. Solana-Madruga, K. N. Alharbi, M. Herz, P. Manuel, J. P. Attfield, *Chem. Commun.*, 2020, **56**, 12574-12577.

- ²¹ E. Solana-Madruga, C. Ritter, O. Mentré, J. P. Attfield, Á. M. Arévalo-López, *J. Mater. Chem. C*, 2022, **10**, 4336-4341.
- ²² M.-R. Li, P. W. Stephens, M. Croft, Z. Deng, W. Li, C. Jin, M. Retuerto, J. P. Hodges, C. E. Frank, M. X. Wu, D. Walker, M. Greenblatt, *Chem. Mater.* 2018, **30**, 4508-4514.
- ²³ E. Solana-Madruga, Á. M. Arévalo-López, A. J. Dos Santos-García, E. Urones-Garrote, D. Ávila-Brande, R. Sáez-Puche, J. P. Attfield, *Angew. Chem. Int. Ed.* 2016, **55**, 9340-9344.
- ²⁴ K. Ji, K. N. Alharbi, E. Solana-Madruga, G. T. Moyo, C. Ritter, J. P. Attfield, *Angew. Chem. Int. Ed.* 2021, **60**, 22248-22252.
- ²⁵ K. Ji, Y. Yuan, G. T. Moy, C. Ritter, J. P. Attfield, *J. Solid State Chem.* 2022, **313**, 123329.
- ²⁶ M. C. Knapp, P. M. Woodward, *J. Solid State Chem.* 2006, **179**, 1076-1085.
- ²⁷ G. King, S. Thimmaiah, A. Dwivedi, P. M. Woodward, *Chem. Mater.* 2007, **19**, 6451-6458.
- ²⁸ G. King, L. M. Wayman, P. M. Woodward, *J. Solid State Chem.* 2009, **182**, 1319-1325.
- ²⁹ C. De, A. Sundaresan, *Phys. Rev. B*, 2018, **97**, 214418.
- ³⁰ R. Shankar P. N., F. Orlandi, P. Manuel, W. Zhang, P. S. Halasyamani, A. Sundaresan, *J. Phys. Chem. C*, 2021, **125**, 6749-6757.
- ³¹ E. Solana-Madruga, Y. Sun, Á. M. Arévalo-López, J. P. Attfield, *Chem. Commun.*, 2019, **55**, 2605-2608.
- ³² E. Solana-Madruga, Á. M. Arévalo-López, A. J. Dos Santos-García, C. Ritter, C. Cascales, R. Sáez-Puche, J. P. Attfield, *Phys. Rev. B* 2018, **97**, 134408.
- ³³ E. Solana-Madruga, P. S. Kearins, K. N. Alharbi, C. T. Lennon, C. Ritter, J. P. Attfield, *Phys. Rev. Materials* 2021, **5**, 054412.
- ³⁴ G. M. McNally, A. M. Arevalo-Lopez, P. Kearins, F. Orlandi, P. Manuel, J. P. Attfield, *Chem. Mater.* 2017, **29**, 8870-8874.
- ³⁵ G. M. McNally, A. M. Arévalo-López, F. Guillou, P. Manuel, J. P. Attfield, *Phys. Rev. Materials* 2020, **4**, 064408.
- ³⁶ P. Kearins, E. Solana-Madruga, K. Ji, C. Ritter, J. P. Attfield, *J. Phys. Chem. C*, 2021, **125**, 9550-9555.
- ³⁷ E. Solana-Madruga, O. Mentré, C. Ritter, C. Aguilar-Maldonado, J. P. Attfield, Á. M. Arévalo-López, *Chem. Commun.*, 2021, **57**, 8441-8444.
- ³⁸ E. Solana-Madruga, C. Ritter, O. Mentré, Á. M. Arévalo-López, *J. Mater. Chem. C*, 2021, **9**, 14916-14920.
- ³⁹ J. B. Goodenough, *Magnetism and the chemical bond*. New York, Wiley, 1963.
- ⁴⁰ Y. Shimakawa, *Inorg. Chem.* 2008, **47**, 8562-8570.
- ⁴¹ Y. Long, *Chin. Phys. B*, 2016, **25**, 078108.
- ⁴² A. A. Belik, R. D. Johnson, D. D. Khalyavin, *Dalton Trans.*, 2021, **50**, 15458-15472.
- ⁴³ W.-t. Chen, M. Mizumaki, H. Seki, M. S. Senn, T. Saito, D. Kan, J. P. Attfield, Y. Shimakawa, *Nat. Commun.* 2014, **5**, 3909.
- ⁴⁴ M. Marezio, P. D. Dernier, J. Chenavas, J. C. Joubert, *J. Solid State Chem.* 1973, **6**, 16-20.
- ⁴⁵ H. S. Horowitz, J. M. Longo, *Mater. Res. Bull.* 1978, **13**, 1359-1369.
- ⁴⁶ B. Bochu, J. Chenavas, J. C. Joubert, M. Marezio, *J. Solid State Chem.* 1974, **11**, 88-93
- ⁴⁷ W.-T. Chen, C.-W. Wang, H.-C. Wu, F.-C. Chou, H.-D. Yang, A. S., M. S. Senn, *Phys. Rev. B*, 2018, **97**, 144102.
- ⁴⁸ T. Locherer, R. Dinnebier, R. K. Kremer, M. Greenblatt, M. Jansen, *J. Solid State Chem.* 2012, **190**, 277-284.
- ⁴⁹ S. V. Ovsyannikov, A. M. Abakumov, A. A. Tsirlin, W. Schnelle, R. Egoavil, J. Verbeeck, G. Van Tendeloo, K. V. Glazyrin, M. Hanfland, L. Dubrovinsky, *Angew. Chem. Int. Ed.* 2013, **52**, 1494-1498.
- ⁵⁰ R. D. Johnson, D. D. Khalyavin, P. Manuel, L. Zhang, K. Yamaura, A. A. Belik, *Phys. Rev. B* 2018, **98**, 104423.
- ⁵¹ F. Mezzadri, M. Calicchio, E. Gilioli, R. Cabassi, F. Bolzoni, G. Calestani, F. Bissoli, *Phys. Rev. B* 2009, **79**, 014420
- ⁵² L. Zhang, N. Terada, R. D. Johnson, D. D. Khalyavin, P. Manuel, Y. Katsuya, M. Tanaka, Y. Matsushita, K. Yamaura, A. A. Belik, *Inorg. Chem.* 2018, **57**, 5987-5998.
- ⁵³ J. Cong, K. Zhai, Y. Chai, D. Shang, D. D. Khalyavin, R. D. Johnson, D. P. Kozlenko, S. E. Kichanov, A. M. Abakumov, A. A. Tsirlin, L. Dubrovinsky, X. Xu, Z. Sheng, S. V. Ovsyannikov, Y. Sun, *Nat. Commun.* 2018, **9**, 2996.
- ⁵⁴ A. A. Belik, *Dalton Trans.*, 2018, **47**, 3209-3217.
- ⁵⁵ B. A. Wechsler, C. T. Prewitt, *Am. Mineral.* 1984, **69**, 176-185.
- ⁵⁶ H. D. Megaw, *Acta Cryst. A*, 1968, **24**, 583-588.
- ⁵⁷ K. Ji, E. Solana-Madruga, M. Amano Patino, Y. Shimakawa, J. P. Attfield, *Angew. Chem. Int. Ed.* 2022, e202203062.
- ⁵⁸ R. E. Newnham, E. P. Meagher, *Mater. Res. Bull.* 1967, **2**, 549-554.

- ⁵⁹ A. J. Dos santos-García, E. Solana-Madruga, C. Ritter, A. Andrada-Chacón, J. Sánchez-Benítez, F. J. Mompean, M. Garcia-Hernandez, R. Sáez-Puche, R. Schmidt, *Angew. Chem. Int. Ed.* 2017, **56**, 4438–4442.
- ⁶⁰ M. R. Li, D. Walker, M. Retuerto, T. Sarkar, J. Hadermann, P. W. Stephens, M. Croft, A. Ignatov, C. P. Grams, J. Hemberger, I. Nowik, P. S. Halasyamani, T. T. Tran, S. Mukherjee, T. S. Dasgupta, M. Greenblatt, *Angew. Chem. Int. Ed.* 2013, **52**, 8406–8410.
- ⁶¹ Á. M. Arévalo-López, E. Solana-Madruga, E. P. Arévalo-López, D. D. Khalyavin, M. Kepa, A. J. Dos santos-García, R. Sáez-Puche, J. P. Attfield, *Phys. Rev. B*, 2018, **98**, 214403.
- ⁶² M. Rong Li, M. Retuerto, P. W. Stephens, M. Croft, D. Sheptyakov, V. Pomjakushin, Z. Deng, H. Akamatsu, V. Gopalan, J. Sánchez-Benítez, F. O. Saouma, J. I. Jang, D. Walker, M. Greenblatt, *Angew. Chem. Int. Ed.* 2016, **55**, 9862–9867.
- ⁶³ M. R. Li, M. Croft, P. W. Stephens, M. Ye, D. Vanderbilt, M. Retuerto, Z. Deng, C. P. Grams, J. Hemberger, J. Hadermann, W.-M. Li, C.-Q. Jin, F. O. Saouma, J. I. Jang, H. Akamatsu, V. Gopalan, D. Walker, M. Greenblatt, *Adv. Mater.* 2015, **27**, 2177–2181.
- ⁶⁴ M.-R. Li, M. Retuerto, D. Walker, T. Sarkar, P. W. Stephens, S. Mukherjee, T. S. Dasgupta, J. P. Hodges, M. Croft, C. P. Grams, J. Hemberger, J. Sánchez-Benítez, A. Huq, F. O. Saouma, J. I. Jang, M. Greenblatt, *Angew. Chem. Int. Ed.* 2014, **53**, 10774–10778.
- ⁶⁵ M.-R. Li, E. E. McCabe, P. W. Stephens, M. Croft, L. Collins, S. V. Kalinin, Z. Deng, M. Retuerto, A. S. Gupta, H. Padmanabhan, V. Gopalan, C. P. Grams, J. Hemberger, F. Orlandi, P. Manuel, W.-M. Li, C.-Q. Jin, D. Walker, M. Greenblatt, *Nat. Commun.* 2017, **8**, 2037.
- ⁶⁶ I. Dzyaloshinsky, *J. Phys. Chem. Solids*, 1958, **4**, 241–255.
- ⁶⁷ S. Geller, J. A. Cape, R. W. Grant, G. P. Espinosa, *Phys. Lett. A*, 1967, **24**, 369–371.
- ⁶⁸ S. V. Ovsyannikov, A. A. Tsirlin, I. V. Korobeynikov, N. V. Morozova, A. A. Aslandukova, G. Steinle-Neumann, S. Chariton, S. Khandarkhaeva, K. Glazyrin, F. Wilhelm, A. Rogalev, L. Dubrovinsky, *Inorg. Chem.* 2021, **60**, 13348–13358.
- ⁶⁹ A. Aimi, T. Katsumata, D. Mori, D. Fu, M. Itoh, T. Kyômen, K.-i. Hiraki, T. Takahashi, Y. Inaguma, *Inorg. Chem.* 2011, **50**, 6392–6398.
- ⁷⁰ J. Ko, C. T. Prewitt, *Phys. Chem. Minerals*, 1988, **15**, 355–362.
- ⁷¹ H. Toyosaki, M. Kawasaki, Y. Tokura, *Appl. Phys. Lett.* 2008, **93**, 072507.
- ⁷² A. M. Arévalo-López, J. P. Attfield, *Phys. Rev. B*, 2013, **88**, 104416.
- ⁷³ Y. Syono, S.-I. Akimoto, Y. Endoh, *Journal of Physics and Chemistry of Solids*, 1971, **32**, 243–249.
- ⁷⁴ R. D. Shannon, C. T. Prewitt, *Acta Cryst. B*, 1969, **25**, 925–946.
- ⁷⁵ G. V. Bazuev, B. G. Golovkin, N. V. Lukin, N. I. Kadyrova, Y. G. Zainulin, *J. Solid. State. Chem.* 1996, **124**, 333–337.
- ⁷⁶ K. Ji, E. Solana-Madruga, A. M. Arevalo-Lopez, P. Manuel, C. Ritter, A. Senyshyn, J. P. Attfield, *Chem. Commun.* 2018, **54**, 12523.
- ⁷⁷ H. L. Feng, Z. Deng, M. Croft, S. H. Lapidus, R. Zu, V. Gopalan, C. P. Grams, J. Hemberger, S. Liu, T. A. Tyson, C. E. Frank, C. Jin, D. Walker, M. Greenblatt, *Inorg. Chem.* 2019, **58**, 15953–15961.
- ⁷⁸ C. Aguilar-Maldonado, E. P. Arévalo-López, C. Ritter, O. Mentré, Á. M. Arévalo-López, *Inorg. Chem.* 2020, **59**, 13128–13135.
- ⁷⁹ B. L. Chamberland, P. S. Danielson, *J. Solid State Chem.* 1971, **3** (2), 243–247.
- ⁸⁰ B. L. Chamberland, L. Katz, *Acta Crystallogr., Sect. B: Struct. Crystallogr. Cryst. Chem.* 1982, **38** (1), 54–57.
- ⁸¹ S. Injac, E. Solana-Madruga, M. Avdeev, H. E. A. Brand, J. P. Attfield, B. J. Kennedy, *Dalton Trans.*, 2020, **49**, 12222–12233.
- ⁸² C. Tassel, Y. Kuno, Y. Goto, T. Yamamoto, C. M. Brown, J. Hester, K. Fujita, M. Higashi, R. Abe, K. Tanaka, Y. Kobayashi, H. Kageyama, *Angew. Chem. Int. Ed.* 2015, **54**, 516–521.